phys. stat. sol. (a) **196**, No. 1, R4–R6 (2003) / **DOI** 10.1002/pssa.200306430

Rapid Research Note

Electronic conductivity in nanostructured TiO_2 films permeated with electrolyte

I. Abayev[1], **A. Zaban**[*,1], **F. Fabregat-Santiago**[2], and **J. Bisquert**[**,2]

[1] Department of Chemistry, Bar-Ilan University, Ramat-Gan 52900, Israel
[2] Departament de Ciències Experimentals, Universitat Jaume I, 12080 Castelló, Spain

Received 5 February 2003, revised 13 February 2003, accepted 14 February 2003
Published online 18 February 2003

PACS 73.30.+y, 73.61.Le, 81.07.Bc

By combining two experimental techniques, electrochemical impedance spectroscopy (EIS) and the coplanar electrodes–gap configuration, we monitored the electronic conductivity in nanoporous TiO_2 in aqueous solution (pH 2) as a function of the electrode potential. As a result of electron accumulation the conductivity varies over more than eight orders of magnitude up to a maximum $\sigma = 3.7 \times 10^{-3}\ \Omega^{-1}\ cm^{-1}$.

Nanoscaled semiconductor materials have become very important for technological developments in photovoltaics, batteries and electrochromic devices. There has been a great deal of recent interest in the electronic conductivity of nanostructured semiconductor materials in different environments [1–4]. In this letter we describe the experimental determination of the electron conductivity in nanocrystalline (nanoporous) TiO_2 in aqueous electrolyte, combining different experimental techniques. When the nanoporous TiO_2 is biased positively the Fermi level lies very far from the conduction band; hence the carrier concentration is low and the conductivity is very low. Here we use EIS as reported recently [4]. If the electrode potential is displaced in the negative direction, the conductivity increases exponentially. Then it is more convenient to determine the conductivity *in situ* utilizing a coplanar configuration (similar to source–bridge–drain transistor setup), in which two halves of the film electrode are separated by a non-conducting gap [5, 6]. The two techniques are complementary and enable measurement of the nanoporous film conductivity over a wide range of Fermi level positions with respect to the conduction band potential.

For the measurement of conductivity in the coplanar configuration, TiO_2 colloids were prepared by hydrolysis of 1:1 solution of titanium (IV) isopropoxide (Aldrich, 99.9%) and 2-propanol in acetic acid (pH = 2). After overnight aging the organic remainders were evaporated at 82 °C followed by a hydrothermal treatment at 250 °C for 13 hours (titanium autoclave, Parr). The production of the TiO_2 slurry was completed by sonication for 5 min, addition of Carbowax (polyethylene glycol compound) to solution and stirring overnight. Using TEM and XRD the TiO_2 particles were characterized as 20 nm in diameter anatase crystals. The TiO_2 slurry was spread on the interdigitated electrodes (ABTECK), dried in air at room temperature and sintered at 450 °C for 30 min. The thickness of the TiO_2 films was $L = 4.5$ μm, measured with Surftest SV 500 profilometer (Mitutoyo Co). The non-conducting gap of the

[*] Corresponding author: e-mail: zabana@mail.biu.ac.il
[**] Corresponding author: e-mail: bisquert@uji.es

 0031-8965/03/19603-00R4 $ 17.50+.50/0

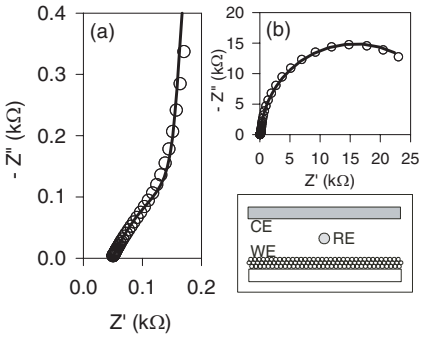

Fig. 1 Experimental setup for measuring the electrochemical impedance and typical impedance spectrum of a nanostructured TiO_2 film. a) High frequency data. b) Low frequency data. Dots are experimental data and lines are the fit of the transmission line model of Ref. [4].

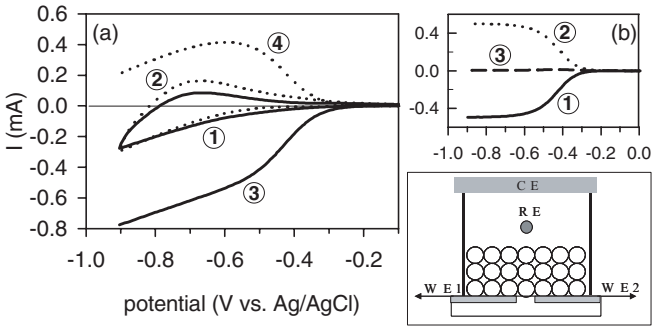

Fig. 2 Scheme of the conductivity measurement in the gap electrode configuration. a) Simultaneous voltammetry scans measured at WE1 (lines) and WE2 (dots). In curves (1), (2), the potential difference between the two electrodes is 0 V, and in (3), (4), −0.010 V. b) Current across the gap vs. the electrode potential (WE1, line, and WE2, dots) obtained by subtracting the baseline current of each WE (at $\Delta V_{WE1-WE2} = 0$) from the currents recorded at $\Delta V_{WE1-WE2} = -0.010$ V. Curve (3) is the difference between (1) and (2).

interdigitated electrode was $t = 5$ μm wide and $d = 14.73$ cm long which provides a high signal to noise ratio. For the EIS sample the process was basically the same with the only difference that the slurry was spread over a normal conducting electrode of area $A = 3.3$ cm^2 [4].

We used the EIS technique in a typical three electrode configuration, Fig. 1, with the TiO_2 film as working electrode (WE), a Pt wire as counter electrode (CE) and an Ag/AgCl electrode as reference electrode (RE). Here the potential of the nanoporous electrode is modulated against the reference in a water solution at pH 2 (H_2SO_4) [4]. Using an equivalent circuit model stated previously [4], it is possible to calculate the transport resistance, R_1, corresponding to electron motion along the axis normal to the substrate and the conductivity is determined as $\sigma = L/(R_1 A)$.

In the coplanar configuration (Fig. 2) the conductivity in pH 2 $HClO_4$ aqueous solution containing 0.2 M $LiClO_4$ was measured using a bi-potentiostat. The TiO_2 film sintered on an interdigitated electrode forms two gold supported nanoporous electrodes that are electrically contacted by the TiO_2 layer present in the gap between the two gold contacts. The measurement is based on a simultaneous scan of the two nanoporous WEs between −0.0 V and −0.9 V (vs. Ag/AgCl) while a small constant potential difference between them is maintained. The current flowing across the gap through the TiO_2 is proportional to its conductivity at each potential. We first record the current–voltage dependence of both electrodes without a potential difference across the gap (Fig. 2a, curves 1 and 2). These voltammograms serve as baselines that account for the contact resistance and the electrode charging [7]. Next we measure the current-voltage dependence of both electrodes in the presence of a small potential difference across the gap. For clarity we present in Fig. 2a (curves 3, 4) the forward scan only, showing that the current increases in one of the electrodes while decreasing in the other one. Subtracting the baseline currents (curves 1, 2) from those obtained in the presence of a bias across the gap (curves 3, 4) provides two curves $i(V)$ of similar shapes but inverse values that correspond to the current flowing across the gap, Fig. 2b (curves 1 and 2). Knowing the cross gap potential, $\Delta V_{WE1-WE2}$, one can use Ohm's law to calculate the resistance across the gap, R_g, as a function of the applied bias voltage, V. Thus the conductivity is calculated as $\sigma = t/(R_g L d)$. Typically, a 10 mV difference is applied across the gap and the resistance values are confirmed by two additional potential differences to ensure that R_g corresponds to the linear region of the $i - \Delta V_{WE1-WE2}$ dependence. We note that over 95% of the current entering the gap from the more negative electrode arrives at the positive electrode. Consequently electron losses in the gap shown in curve 3 of Fig. 2b may be neglected.

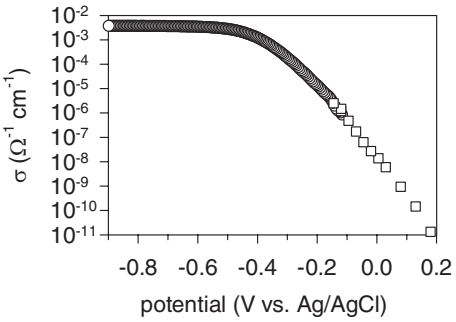

Fig. 3 Electronic conductivity in nanostructured TiO_2 electrodes in solution at pH 2 as a function of the electrode potential. The square points were determined by EIS as indicated in Fig. 1. The circle points were determined in a coplanar configuration as indicated in Fig. 2. The EIS data have been shifted +80 mV to account for the difference of the activity of solutions used in the two measurements.

The results of the electron conductivity, σ, in nanoporous TiO_2 electrodes, combining the two measurements are shown in Fig. 3. The match of results of the two techniques is excellent, specially concerning the slope in the region of overlap. This slope is very important, because it indicates the potential-dependence of σ (the absolute values may be subjected to a certain error due to indeterminacy in the geometrical factors).

The overall behavior of the conductivity shows two domains separated by the crossover at –0.5 V vs. Ag/AgCl. This potential corresponds to the lower edge of the conduction band of anatase TiO_2 at pH 2 [7]. Between 0.2 and –0.5 V (Ag/AgCl), Fig. 3 shows in a direct fashion the correlation of the electron conductivity to the increasing electron accumulation induced by the potential. Thus variation of σ can be understood in terms of the progressive displacement of the Fermi level towards the conduction band, which is related to the photovoltage mechanism in dye sensitized solar cells. In this region the dependence of σ on the bias potential is close to $\exp(-eV/k_BT)$, where k_BT/e is the thermal voltage, i.e. the variation is near to 60 mV/decade. On the other hand, at potentials more negative than –0.5 V (Ag/AgCl) a saturation of the conductivity is observed, probably due to a state of Fermi level pinning.

In the case of sintered metal-oxide semiconductor nanoparticles (ca. 10 nm diameter) electrode, mobile ions in solution can screen the electrical fields beyond the nanoscopic dimension, so that the electron transport occurs predominantly by diffusion. Therefore the conductivity in Fig. 3 corresponds to diffusive electron transport and can be written $\sigma = ne\mu$, where n is the carrier density and the mobility relates to the diffusion coefficient as $\mu = eD/k_BT$. The measured value of conductivity in the saturation range is $\sigma = 3.7 \times 10^{-3}\ \Omega^{-1}\,cm^{-1}$. Assuming $n = 10^{20}\ cm^{-3}$ in this range (as confirmed by voltammetry [7]) the average electron mobility and diffusion coefficient take the values $\mu = 2.3 \times 10^{-4}\ cm^2/Vs$ and $D = 6.0 \times 10^{-6}\ cm^2/s$, respectively. These estimated values are similar to those reported by Solbrand et al. [2] in dye-sensitized solar cells ($D = 3–8 \times 10^{-6}\ cm^2/s$). The explanation of the conductivity features in Fig. 3 in terms of a transport model in which the exponential distribution of traps [7] plays a central role, is currently being developed.

Acknowledgements We acknowledge the support of this work by the Israeli Ministry of Science and the Fundació Caixa Castelló.

References

[1] T. Dittrich, E. A. Lebedev, and J. Weidmann, phys. stat. sol. (a) **167**, R5 (1998).
[2] A. Solbrand, A. Henningsson, S. Sodergren, H. Lindstrom, A. Hagfeldt, and S.-E. Lindquist, J. Phys. Chem. B **103**, 1078 (1999).
[3] R. Könenkamp, Phys. Rev. B **61**, 11057 (2000).
[4] F. Fabregat-Santiago, G. Garcia-Belmonte, J. Bisquert, A. Zaban, and P. Salvador, J. Phys. Chem. B **106**, 334 (2002).
[5] E. A. Meulenkamp, J. Phys. Chem. B **103**, 7831 (1999).
[6] A. L. Roest, J. J. Kelly, D. Vanmaekelbergh, and E. A. Meulenkamp, Phys. Rev. Lett. **89**, 036801 (2002).
[7] F. Fabregat-Santiago, I. Mora-Seró, G. Garcia-Belmonte, and J. Bisquert, J. Phys. Chem. B **107**, 758 (2003).